An Experimental Investigation of the Shock Layer Surrounding a Sphere in Supersonic Flow

J. XERIKOS* AND W. A. ANDERSON†
Douglas Aircraft Company, Inc., Santa Monica, Calif.

An experimental study of the flow properties in the transonic and supersonic regions of the flow field surrounding a sphere was conducted in order to provide more definitive flow-field data for evaluating current analytical blunt-body methods. In particular, results were compared with the predictions of the one-strip direct integral method in order to determine the most valid form of the integrand approximations employed. The tests were conducted at nominal Mach numbers of 3, 4, and 5. Static and total pressure measurements were taken across the shock-layer region. A mechanized probe was employed which enabled a complete shock-layer pressure profile to be determined during a single tunnel run. Probe alignment at each station was matched to flow inclination values predicted by the integral method. Surface static pressures were also taken. In order to minimize the disturbing effect of the probe on transonic shock-layer properties, a 14.9-in.-diam sphere was employed in order to increase the scale of the flow relative to probe size. Shock-shape data were obtained through the use of shadowgraphs and schlieren photographs.

Introduction

THE continuing interest and activity in blunt-body analyses has motivated a number of experimental investigations that have dealt largely with the measurement of shock-wave shapes and surface pressure distributions.[1–6] Determination of shock-layer flow properties in the transonic zone has been accomplished primarily through the use of optical methods, e.g., ballistic range interferometric measurements[7] and sonic line location technique using a shock generating probe.[8] Since the theoretical blunt-body methods provide characteristics starting data for computing the remainder of the supersonic or hypersonic flow field, stringent accuracy requirements must be placed on the predicted distribution of flow properties across the shock layer. The necessity for accuracy is particularly critical for configurations with small nose blunting since the characteristics calculation must be carried out over a distance corresponding to a large number of body nose radii.

The present investigation was conducted with the principal aim of providing shock-layer data not currently available for further evaluation of theoretical methods. A secondary, more specific goal was to resolve questions arising in connection with the formulation of the integral method through the use of experimental evidence. It is hoped that the data and experience gained in the present study will provide a basis for an extended investigation in the hypersonic regime.

Experimental Procedure

Test Facility

The tests were conducted in the Douglas Aircraft Aerophysics Laboratory trisonic 4-ft tunnel (Mach number is continuously variable from 0.2 to 5.0). The tunnel is a blowdown to atmosphere facility with running times on the order of 40–60 sec. The Mach number in the 4-ft square test section ($4 \times 4 \times 6$ ft) is uniform within 0.006 with a flow angularity not exceeding 0.1°. Nominal values of stagnation pressure, stagnation temperature, and Reynolds number based on sphere diameter are given in Table 1 for the three test Mach numbers.

Presented as Preprint 64-429 at the 1st AIAA Annual Meeting, Washington, D. C., June 29–July 2, 1964. The authors would like to thank L. A. Kay and D. T. Lloyd for their able assistance in the planning and conduct of the experiment. This work was supported by the Douglas Independent Research and Development Program.

* Chief, Fluid Mechanics Research Section. Member AIAA.
† Member, Fluid Mechanics Research Section. Member AIAA.

Model Description

The basic model configuration consisted of a 14.9-in.-diam sting-mounted sphere as shown in Fig. 1. The sphere was fabricated from a solid ingot of aluminum with the final process involving anodizing of the polished surface. All pressure transducers (differential pressure type: Statham PM-131) as well as a wafer valve pressure switch were located within the model (Fig. 2), thus reducing the lag time in recording pressures. Whereas the traversing and centerline probes employed separate transducers, model surface and "hatchet" static pressure readings were scanned using the wafer valve switch and associated transducers. A Sanborn dynamic recorder was used for visual monitoring of the selected pressure measurements during the test runs.

Surface Pressures

Nine static pressure orifices were located at 10° intervals from $\theta = 10°$ to $\theta = 90°$. An additional pressure tap was

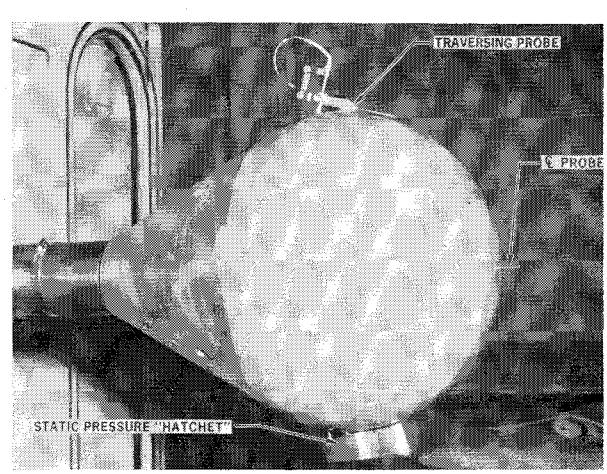

Fig. 1 Model exterior.

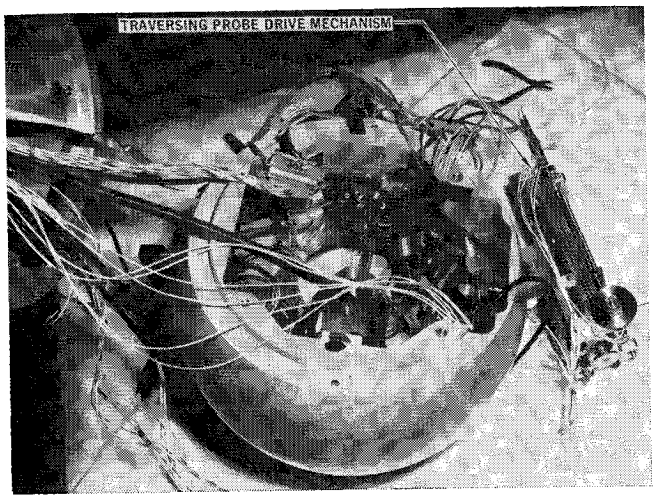

Fig. 2. Model interior.

located at $\theta = -30°$ in order to check alignment of the model. The entire model was pitched a total of 10° in 2° increments such that a dense distribution of data points was obtained. Owing to the short lag time in recording pressures, a complete range of pitch positions was covered during one or two runs.

Shock-Layer Pressures

Static and total pressure measurements were taken across the shock-layer region along radial lines corresponding to $\theta = 45°$, 60°, and 75°. The traversing probe mechanism accomodated either a total pressure or static pressure probe on a given run. Use of a single pitot-static probe (visible in Fig. 1) was ruled out during the testing in order that total and static pressure readings be taken at the same point in the flow field and probe dimaeter be kept to a minimum. The traversing mechanism was mechanically programmed to stop at intervals of $0.1\delta_{theor}$ where δ_{theor} = distance between body and shock, measured normal to the body surface as predicted by the one-strip integral method. In addition, the probe alignment at each stop was matched to the theoretical (integral method) flow inclination values. Nine "stop rails" and cams (see Fig. 3) corresponding to the various combinations of three test Mach numbers and three angular positions θ were necessary in order to attain the desired probe movement. This movement was such that the tip of the total pressure probe and the four circumferentially located holes in the static probe traced coincident paths along the specified radial lines. It should be noted that the use of preset static probe angular alignment introduced a weak coupling between theoretical and experimental results.

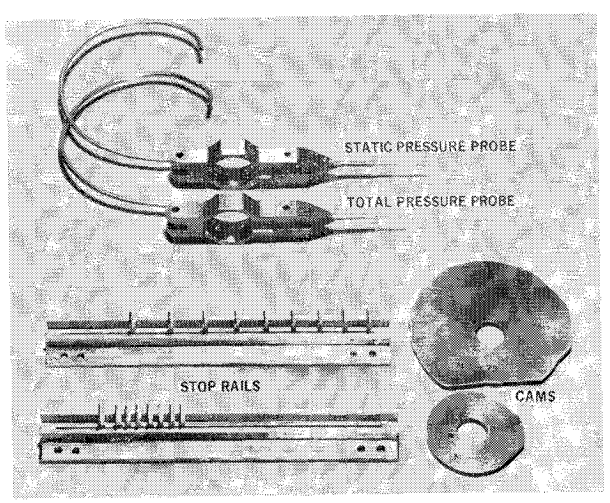

Fig. 3 Model details.

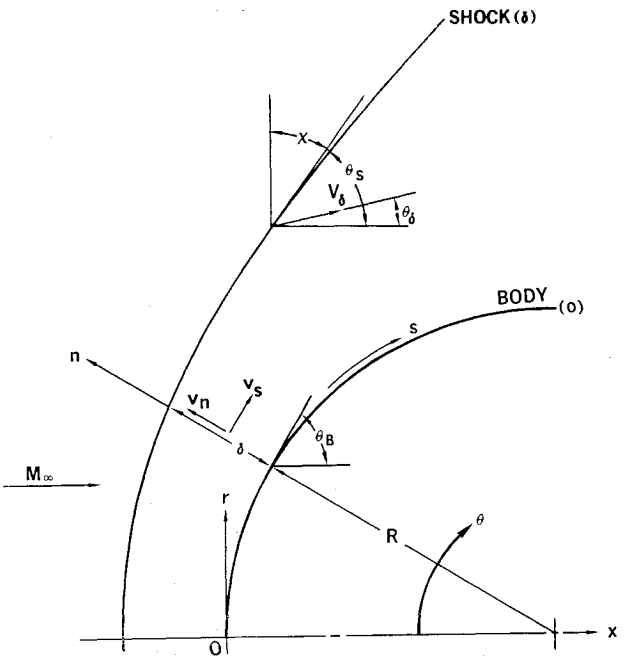

Fig. 4 Coordinate system and nomenclature.

Additional Instrumentation

The static pressure "hatchet" consisted of a sharp edge flat plate with a row of eight static pressure orifices aligned in the radial direction. This device could be manually set at various positions within the shock layer with the orifices always remaining along one of the specified radial lines.

The centerline total pressure probe was instrumented to provide continuous measurement of total pressure and corresponding probe position.

Flow Visualization

Use was made of both parallel light shadowgraph and schlieren optical systems to record visual shock-layer phenomena. The 30-in. schlieren system is capable of recording

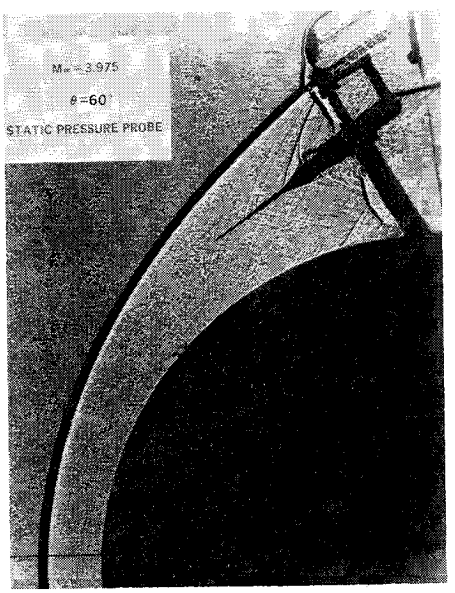

Fig. 5 Typical shadowgraph.

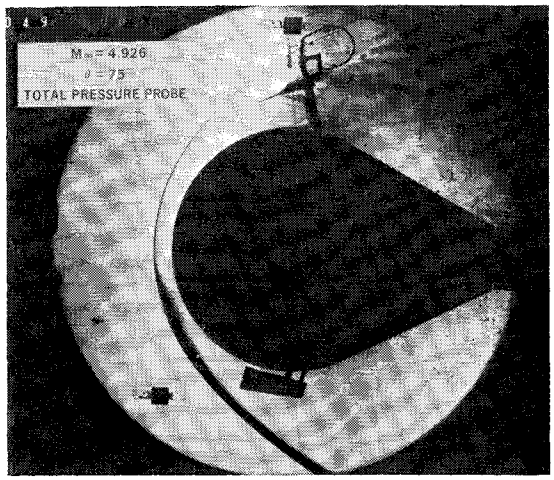

Fig. 6 Typical schlieren photograph.

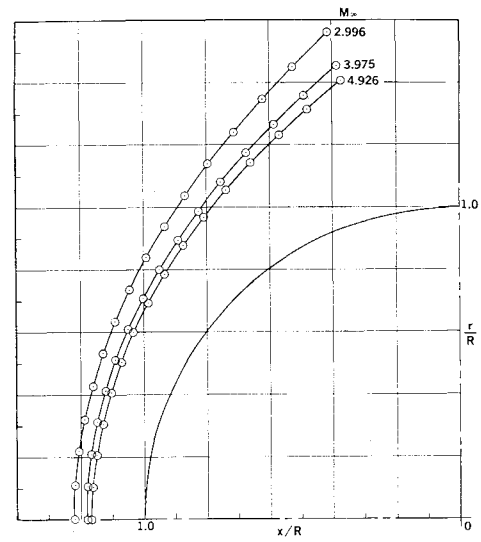

Fig. 7 Experimental shock shapes.

single-frame photographs (70mm negative) at rates up to 5/sec. During test runs involving the traversing probe, a schlieren photograph was taken at each stop position as the probe crossed the shock layer and eventually penetrated the bow shock. This procedure provided a visual check of probe position and alignment. Full scale shadowgraphs were also taken using an 11 × 14-in. film holder mounted on the tunnel window. Only one shadowgraph, however, could be taken during a single run.

Discussion of Integral Method

One of the factors that motivated the present investigation involved a question concerning the formulation of the integral method which could only be satisfactorily resolved through consideration of experimental evidence. Therefore, a brief discussion of the analysis is given below in order to identify the point in question.

An initial step in the integral method requires that the governing partial differential equations be represented in "divergence" form, e.g.,

$$(\partial F/\partial s) + (\partial G/\partial n) + H = 0$$

where (s, n) are body-oriented, curvilinear coordinates (see Fig. 4). Subsequent integration with respect to n necessitates approximation of the functions F and H in terms of, for example, polynomials in n with s-dependent coefficients. A linear relationship is ordinarily employed in the one-strip formulation.

An additional arbitrariness arises owing to the fact that several combinations of the governing equations will yield valid ordinary differential equations, which, for an increasing number of strips (and a correspondingly more accurate approximation for the flow properties across the shock layer), should tend to produce the same result. However, a marked difference in results exists for the one-strip approximation. Table 2 summarizes the pertinent relations corresponding to two representative formulations. As may be seen, different functions are being approximated in each case. It should be noted that formulation *Ia* corresponds to the original, widely employed Belotserkovskii analysis. A more general form of the modified continuity equation is also presented

Table 1 Nominal test conditions

M_∞	p_{t_∞} psia	T_{t_∞}, °F	Re
2.996	65	60	$15 \cdot 10^6$
3.975	140	55	
4.926	285	180	

Ib which may be used to describe, for example, a flow process involving a gas in thermodynamic equilibrium. This form reduces to the original version of the equation *Ia* when perfect gas relations are employed.

The "continuity" formulation (II) is not restricted to a particle isentropic process (i.e., constant entropy along streamlines) and would initially appear to be a logical choice for a real gas analysis involving nonequilibrium processes. However, since the perfect gas numerical results corresponding to use of the two formulations differed significantly, an evaluation based on direct comparison with experimental data was felt to be necessary. Although the test conditions did not correspond to the hypersonic real gas regime, it appeared reasonable to expect that a valid theoretical analysis should yield accurate results in the supersonic regime.

Discussion of Experimental Results

The experimental data are presented in Figs. 7–21 with the corresponding theoretical predictions of the one-strip integral method.[9] Additional theoretical results are included in the

Table 2 Summary of integral method relations

PARTIAL DIFFERENTIAL EQUATION IN DIVERGENCE FORM $\frac{\partial F_i}{\partial s} + \frac{\partial G_i}{\partial n} + H_i = 0$	YIELDS ORDINARY DIFFERENTIAL EQUATION FOR: (ONE-STRIP APPROXIMATION) F_i	H_i		DIVERGENCE FORM OBTAINED BY TAKING:
MODIFIED n-MOMENTUM	$r\rho v_S v_n$	$-\frac{r}{R}(p + \rho v_S^2)$ $-p(1 + \frac{n}{R})\cos\phi_B$	χ	$v_n F_C + r_p F_{M_n}$
(a) MODIFIED CONTINUITY	$r\rho\phi^{\frac{1}{\gamma-1}} v_S$	0	v_{S_0}	$\phi^{\frac{1}{\gamma-1}}(F_C + \frac{r_p}{\phi(\gamma-1)} F_\phi)$
(b) ENTROPY-CONTINUITY	$r\rho e^S v_S$	0		$e^S(F_C + r_p F_S)$
II CONTINUITY	$r\rho v_S$	0		F_C

NOTATION

$S = \frac{1}{(\gamma-1)} \ln e\phi$, $\phi = (p/p_{t_\infty})/(\rho/\rho_{t_\infty})^\gamma$ (ISENTROPIC PROCESS, PERFECT GAS)

$F_C = \frac{\partial}{\partial s}(r\rho v_S) + \frac{\partial}{\partial n}[r(1 + \frac{n}{R})\rho v_n]$

$F_{M_n} = v_S \frac{\partial v_n}{\partial s} + (1 + \frac{n}{R}) v_n \frac{\partial v_n}{\partial n} - \frac{v_S^2}{R} + \frac{1}{\rho}(1 + \frac{n}{R})\frac{\partial p}{\partial n}$

$F_\phi = v_S \frac{\partial \phi}{\partial s} + (1 + \frac{n}{R}) v_n \frac{\partial \phi}{\partial n}$

$F_S = v_S \frac{\partial S}{\partial s} + (1 + \frac{n}{R}) v_n \frac{\partial S}{\partial n}$

} USE OF EITHER RELATION IMPOSES RESTRICTION TO PARTICLE ISENTROPIC FLOW

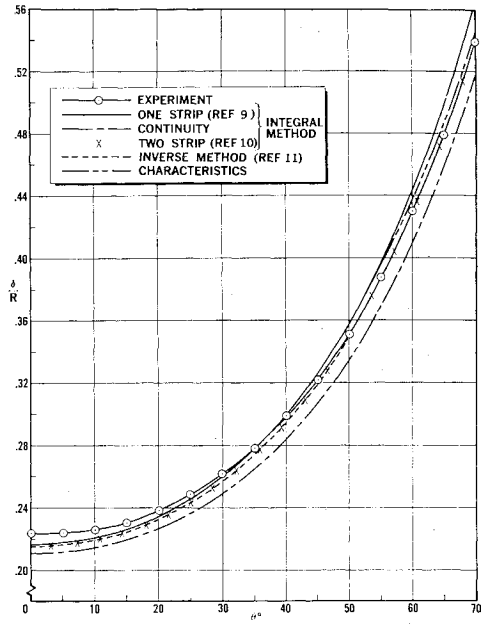

Fig. 8 Comparison of shock shapes: $M_\infty = 2.996$.

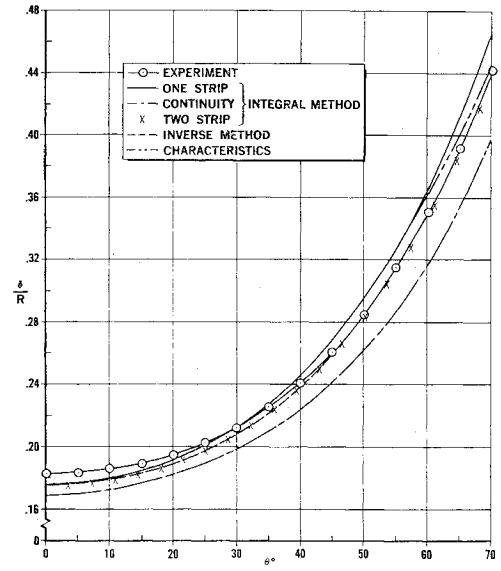

Fig. 9 Comparison of shock shapes: $M_\infty = 3.975$.

presentation of the experimental shock shapes. The accuracy of the analytical methods for $\theta = 45°$ holds particular significance since the input line for the method of characteristics typically lies in the zone $45° < \theta < 50°$.

Shock-Wave Shapes

The experimental shock data presented in graphical form are based on direct measurement of full scale shadowgraphs, e.g., Fig. 5. The accuracy of the data is basically dictated by the following considerations: 1) resolution of shock and body images, 2) ability of optical system to produce a parallel light beam across the test section, and 3) displacement of body image due to refraction caused by density changes across the shock layer. The resolution was sufficient to limit measurement errors to $\Delta\delta/R \simeq 0.001$. Use of a reference dimension device indicated negligible magnification of the image. Although the film holder was mounted on the test section window to help minimize the displacement effect, this effect appears to be the main source of error.

Supplementary shock data were provided by schlieren photographs. Although not subject to image distortion in principle, the schlieren shock and body images were not as uniformly sharp as the shadowgraphs. A representative example is shown in Fig. 6. Schlieren measurement errors were estimated to be of the order of $\Delta\delta/R \simeq 0.003$. Table 3 presents a comparison of data obtained by both optical techniques. The results differ by 2–6% with the maximum differences occurring in the measurement of the detachment distance ($\theta = 0°$).

An attempt was made to obtain additional shock-shape measurements through use of the position calibrated pressure probe located at the sphere stagnation point. A continuous pressure trace on a Sanborn recorder failed to identify a distinct pressure step as the shock was pierced. This failure was largely due to the continuous distortion of a portion of the bow shock as the probe approached from the subsonic zone. In contrast, the traversing probe used to obtain shock profiles displayed steep pressure steps as the shock was penetrated in the supersonic zone. However, this probe was not instrumented with a position recording device. Unfortunately, the maximum pitch angle of the model support ($\alpha = 25°$) did not allow the probe to pierce the bow shock above the shock sonic point.

The graphic results that are all derived solely from shadowgraph measurements are presented in both (x, r) coordinates in Fig. 7, and δ/R vs θ plots in Figs. 8–10. The latter graphs include theoretical data from the one-strip and two-strip[10] (available at $M_\infty = 3$ and 4 only) integral methods, an inverse method[11] (up to $\theta = 48°$), and characteristics results based upon one-strip data input at $\theta = 50°$. The "inverse" results shown are in substantial agreement with those of other investigators employing this method.[12]

With the possible exception of the "continuity" formulation (II), the theoretical results compare favorably with the shock data. The inverse method predictions appear to correspond most closely to the two-strip results. The one-strip (I) shock shape extended by the method of characteristics tends to converge toward the experimental data. It should be noted that the schlieren data are in better agreement with the theoretical predictions in the stagnation region.

The "continuity" shock shape tends to diverge significantly from the experimental data with increasing Mach number indicating the undesirability of this formulation for hypersonic analyses. This theoretical shock behavior is also accompanied by an overly rapid drop in surface pressure, causing an upstream shift in the location of the body sonic point.

Surface Pressure Distributions

Surface pressure data for $M_\infty = 2.996$, 3.975, 4.926 are presented in Figs. 11–13, respectively. A model free of

Table 3 Comparison of schlieren (δ_{SC}) and shadowgraph (δ_{SH}) shock data

	$M_\infty = 2.996$		$M_\infty = 3.975$		$M_\infty = 4.926$	
θ	δ_{SC}/R	δ_{SH}/R	δ_{SC}/R	δ_{SH}/R	δ_{SC}/R	δ_{SH}/R
0°	0.213	0.223	0.173	0.183	0.156	0.165
45°	0.315	0.322	0.250	0.260	0.229	0.237
60°	0.422	0.430	0.343	0.351	0.309	0.315
75°	0.600	0.614	0.490	0.502	0.442	0.452

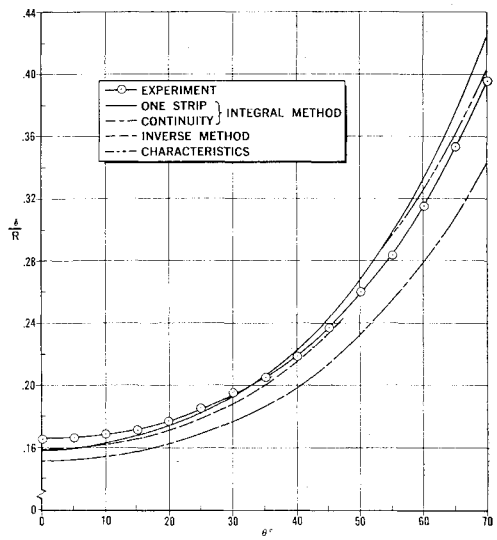

Fig. 10 Comparison of shock shapes: $M_\infty = 4.926$.

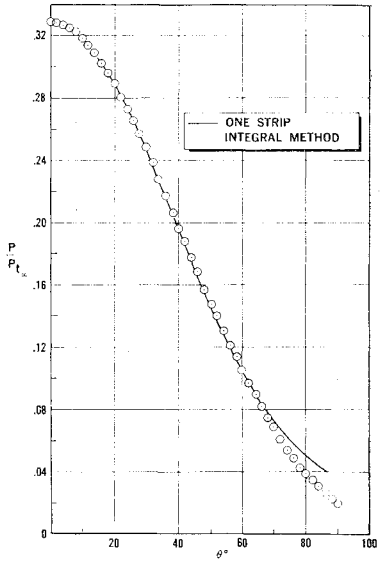

Fig. 11 Surface pressure distribution: $M_\infty = 2.996$.

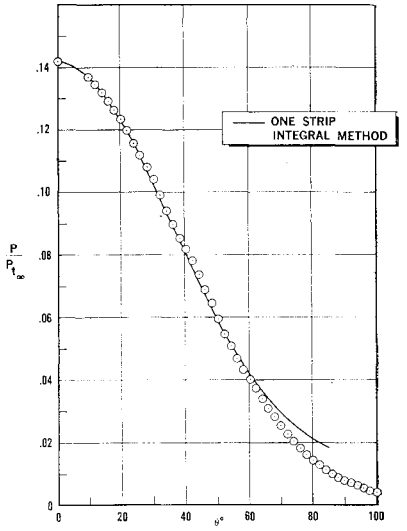

Fig. 12 Surface pressure distribution: $M_\infty = 3.975$.

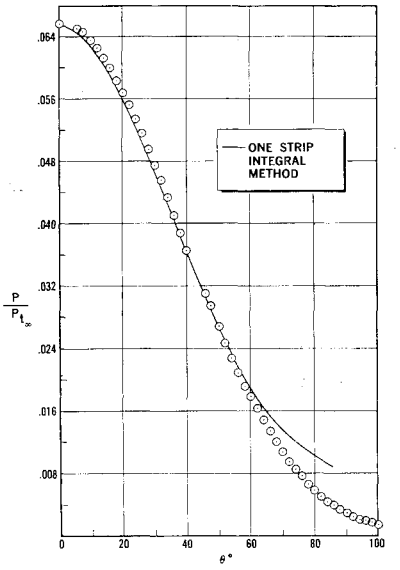

Fig. 13 Surface pressure distribution: $M_\infty = 4.926$.

probes was employed when taking surface pressure measurements. Because of the sensitivity of the reference parameter p_{t_∞} to changes in M_∞, recomputation of the theoretical data at the exact freestream Mach number was necessary to obtain a valid comparison of results.

The theoretical prediction is satisfactory up to the sonic point with a gradual divergence taking place in the supersonic region. The surface pressure data indicate a decrease in accuracy of the one-strip integral method with increase in Mach number.

Shock-Layer Pressure and Mach Number Distributions

Static pressure, isentropic total pressure, and Mach number profiles taken at $\theta = 45°, 60°, 75°$ are displayed in Figs. 14–21. The theoretical profiles were derived using exact inviscid shock and body gradients in the n direction based on the variation of flow properties in the s direction given by the integral method. The results are plotted in terms of the nondimensional distance n/δ measured normal to the surface of the sphere.

In all cases, the experimentally measured shock wave was closer to the body than was the theoretical shock. As a result, the traversing probe pierced the shock wave between the ninth and tenth stop positions, i.e., between 0.9 and $1.0\delta_{\text{theor}}$. This was confirmed by schlieren and shadowgraph photographs as well as by the trace on the Sanborn recorder. Therefore, the experimental points do not fall exactly on the

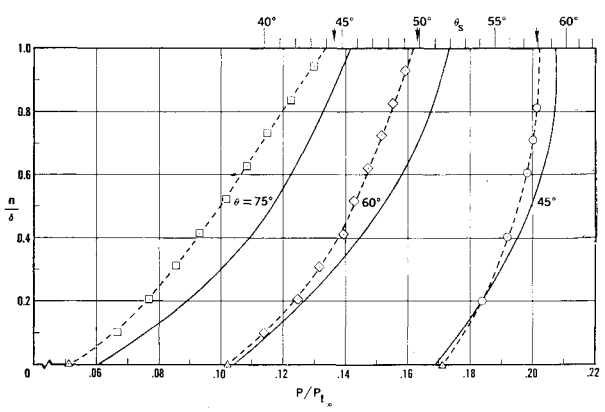

Fig. 14 Shock-layer static pressure profiles: $M_\infty = 2.996$.

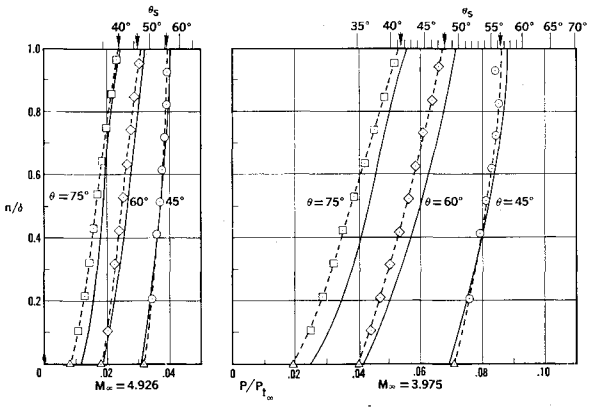

Fig. 15 Shock-layer static pressure profiles: $M_\infty = 3.975$, 4.926.

values of $n/\delta = 0.1, \ldots, 1.0$ but are shifted in proportion to $n \times \delta_{theor}/\delta_{exper}$.

The data reduction procedure was relatively straightforward. Static and pitot probe data were used to determine the local Mach number through use of the Rayleigh pitot equation, thus enabling the subsequent evaluation of the isentropic total pressure.

Although the shock-layer data are largely self-explanatory, several specific comments are in order. The dashed curves drawn through the experimental results are intended to depict general experimental trends relative to the shapes of the theoretical profiles. This comparison is favorable in the majority of cases; an advantage is thus indicated in use of the gradient method in establishing shock-layer profiles. An increase in tunnel Mach number occurred during the $M_\infty = 4.926$, $\theta = 60°$, total pressure run. This increase is reflected in an erratic shift in the data as indicated in Fig. 18.

Deviation of the curves at $n/\delta = 0$ primarily reflected the error in predicting surface pressure distributions, whereas deviation at $n/\delta = 1$ reflected the error involved in predicting the shock shape. The scale at the top of Figs. 14 through 18 was included to indicate the sensitivity of the parameters $(p/p_{t_\infty})_{shock}$ and $(p_t/p_{t_\infty})_{shock}$ to small changes in θ_s. Measurement of the shock-wave slope from shadowgraphs and subsequent calculation of post-shock values of static and total pressure (indicated by a vertical arrow on the θ_s scale) provided a consistency check on the field data. An additional check was afforded by the requirement that the locus of the experimental points fare smoothly into the independently measured surface total and static pressures.

The static pressure "hatchet" did not provide satisfactory data because of a combination of instrumentation difficulties and evidence of self-induced flow interference when mounted near the surface of the sphere. As a result, pressure readings

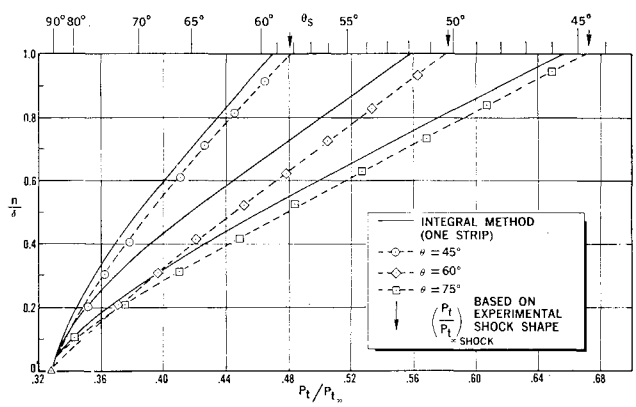

Fig. 16 Shock-layer isentropic total pressure profiles: $M_\infty = 2.996$.

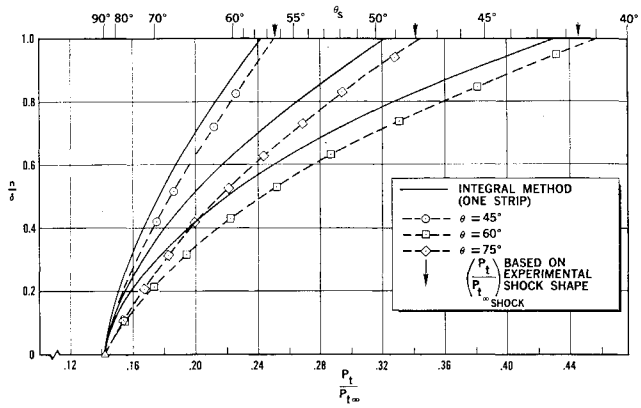

Fig. 17 Shock-layer isentropic total pressure profiles: $M_\infty = 3.975$.

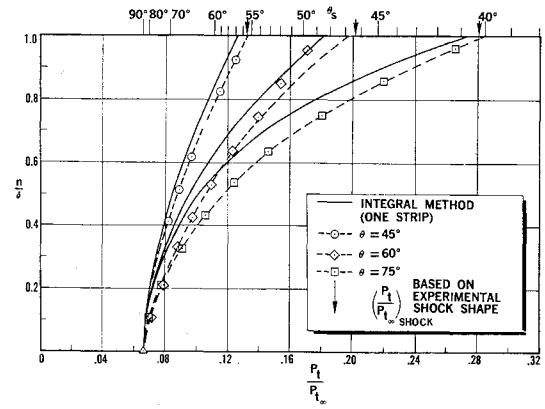

Fig. 18 Shock-layer isentropic total pressure profiles: $M_\infty = 4.926$.

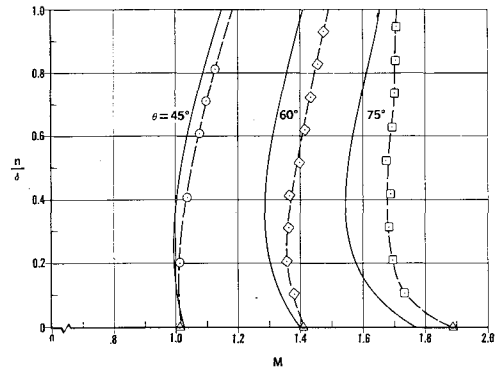

Fig. 19 Shock layer Mach number profiles: $M_\infty = 2.996$-.

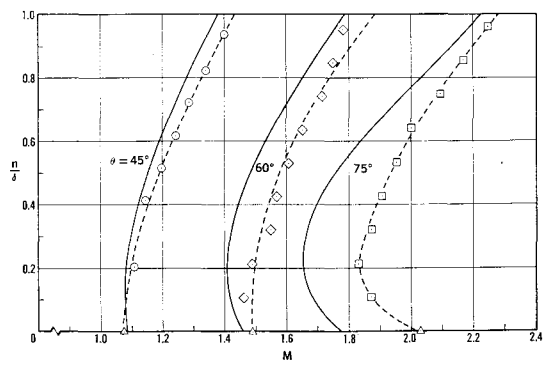

Fig. 20 Shock-layer Mach number profiles: $M_\infty = 3.975$.

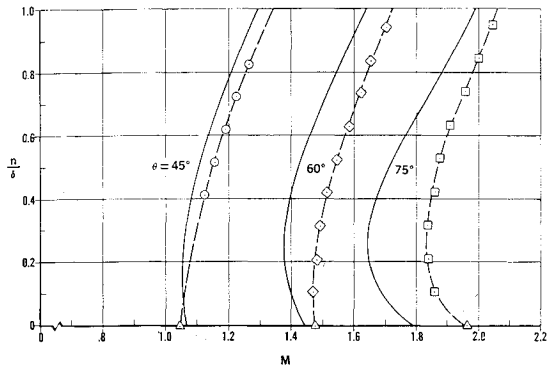

Fig. 21 Shock layer Mach number profiles: $M_\infty = 4.926$.

were erratic and could not be used to establish smooth static pressure profiles independently. However, the pressures measured were in partial agreement with the static probe measurements. Time limitations prevented a definitive evaluation of the usefulness of this device in making shock-layer measurements.

Conclusions

The main test objective, namely, that of obtaining accurate shock-layer pressure profiles, was essentially met on the basis of critical examination of the experimental data. While no gross deviations from predicted theoretical trends were indicated (or expected), an additional quantitative basis for evaluating blunt-body methods was established.

Use of a "continuity" integral method formulation led to a description of the shock and body parameters which became progressively inaccurate with increase in Mach number.

Further study is needed to establish the feasibility of determining shock-wave profiles through nonoptical devices such as the probe used in the present investigation.

References

[1] Baer, A. L., "Pressure distributions on a hemisphere cylinder at supersonic and hypersonic Mach numbers," von Karman Gas Dynamics Facility, ARO, Inc. Rept. AEDC-TN-61-96 (August, 1961); also Armed Services Technical Information Agency ASTIA AD-261 501 (August 1961).

[2] Boison, J. C. and Curtiss, H. A. "An experimental investigation of blunt body stagnation point velocity gradient," ARS J. **29**, 130-135 (February 1959).

[3] Kuehn, D. M., "Experimental and theoretical pressures on blunt cylinders for equilibrium and nonequilibrium air at hypersonic speeds," NASA TN D-1979 (November 1963).

[4] Oliver, R. E., "An experimental investigation of flow over simple blunt bodies at a nominal Mach number of 5.8," Guggenheim Aeronautical Lab., California Institute of Technology Memo. 26 (June 1955).

[5] Vas, I. E., Bogdonoff, S. M., and Hammitt, A. G., "An experimental investigation of the flow over simple two-dimensional and axial symmetric bodies at hypersonic speeds," Princeton University Rept. 382 (June 1957).

[6] Osborne, W. K. and Crane, J. F. W., "Measurement of the sonic line, bow shock wave shape and stand-off distance for blunt-nosed bodies at $M = 6.8$," Royal Aircraft Establishment TN AERO.2707 (August 1960); also Armed Services Technical Information Agency ASTIA AD-245 832.

[7] Sedney, R. and Kahl, G. D., "Interferometric study of the blunt body problem," Ballistic Research Labs. Rept. 1100 (April 1960).

[8] Kendall, J. M., "Experiments on supersonic blunt-body flows," California Institute of Technology Progress Rept. 20-372 (February 1959).

[9] Xerikos, J. and Anderson, W. A., "A critical study of the direct blunt body integral method," Douglas Aircraft Co., Inc. Rept. SM-42603 (December 28, 1962).

[10] Belotserkovskii, O. M., "Calculation of flows past axially symmetric bodies with detached shock wave," Computer Center, Academy of Sciences, Moscow (1961).

[11] Batchelder, R. A., "An inverse method for inviscid ideal gas flow fields behind analytical shock shapes," Douglas Aircraft Co., Inc. Rept. SM-42588 (July 1963).

[12] Van Dyke, M. D. and Gordon, H. D., "Supersonic flow past a family of blunt axisymmetric bodies," NASA Rept. 1 (1959).